Vacancy Clusters on Surfaces of Au Nanoparticles Embedded in MgO

Jun Xu,[1] A. P. Mills, Jr.,[2] A. Ueda,[3] D. O. Henderson,[3] R. Suzuki,[4] and S. Ishibashi[4]
[1]*Oak Ridge National Laboratory, P.O. Box 2008, Oak Ridge, Tennessee 37831-6142*
[2]*Bell Laboratories, Lucent Technologies, 600 Mountain Avenue, Murray Hill, New Jersey 07974*
[3]*Chemical Physics Laboratory, Physics Department, Fisk University, 1000 17th Avenue North, Nashville, Tennessee 37208*
[4]*Electrotechnical Laboratory, 1-1-4 Umezono, Tsukuba, Ibaraki 305, Japan*
(Received 20 January 1999; revised manuscript received 2 September 1999)

MeV implantation of gold ions into MgO(100) followed by annealing is a method to form gold nanoparticles for obtaining modified optical properties. We show from variable-energy positron spectroscopy that clusters of 2 Mg and 2 O vacancies (v_4) are attached to the gold nanoparticle surfaces within the projected range (R_p). We also find that v_4 vacancy clusters are created at depths less than R_p, and extend into the region greater than R_p due to damage induced by knock-on collisions.

PACS numbers: 61.72.Ji, 78.70.Bj

As studies of nanoparticles gain attention [1], understanding of the surface structures of nanoparticles becomes more urgent since the surface-to-bulk ratio is much larger at nanometer scales than it is for macroscopic samples. In this Letter we show that positron spectroscopic measurements, combined with detailed electronic structure calculations which include the effect of the positron [2], can provide new information about defect structures on the surfaces of colloidal gold particles embedded in crystalline MgO. We have discovered a correlation between vacancy clusters and Au nanoparticles. In fact, the Au implants are not visible by the positron probe until they form nanoclusters that are associated with vacancies.

Implantation [3] of metal ions into single crystal MgO followed by annealing creates colloidal metal particles with a diameter of a few nm [4,5]. These composite materials, consisting of metal colloids in a dielectric host, have new optical properties, such as a high optical nonlinearity associated with the surface plasmon or Mie resonances of the colloidal particles [6,7]. The implantation process, of course, generates vacancy-type defects, such as F centers (oxygen vacancies occupied by two electrons) and V centers (magnesium vacancies), as well as interstials. These defects can become associated with the interface between the nanoparticle and host material during the heat treatment processes. On the other hand, such interfacial defects can affect the apparent nanoparticle bulk properties since the surface-to-bulk ratio becomes very large for nanoscale particles. An understanding of the defect structure of nanoparticle surfaces is then essential in explaining the properties of nanoscale composites.

Au nanoparticles formed in Au^+ implanted MgO can be detected by the surface plasmon resonance [4,5] and observed directly by transmission electron microscopy [8]. Some vacancy structures can be measured with limited sensitivity using optical spectroscopy. For example, isolated F centers and F_2 centers can be studied in optical absorption spectra [9]. Depth profiling using variable energy positron spectroscopy [10] is uniquely sensitive for the detection of vacancy clusters at low concentrations, since injected positrons are preferably trapped in these defect sites. In this Letter we use both the positron lifetime spectroscopy and Doppler broadening of annihilation radiation techniques to specify that there are significant numbers of vacancy clusters located on the surfaces of Au nanoparticles embedded in MgO.

MgO(100) single crystals were obtained from two vendors (Harrick Scientific and Commercial Crystal Laboratory), which have two major impurities: Fe^{3+} at 100 ppm and Al^{3+} at 40 ppm. The samples were implanted with 1.1 MeV gold ions at doses of 1, 3, 6, and 10×10^{16} Au ions/cm^2 in the Oak Ridge National Laboratory Surface Modification and Characterization (SMAC) research facility. The depth profiles of gold concentration were measured by Rutherford backscattering spectroscopy (RBS), using 2.3 MeV α particles, which show that the Au ions are primarily located in the range of 0.16–0.4 μm. The implanted samples were found to remain crystalline during implantation. Thermal annealing was carried out at a temperature of 1200 °C in either an inert, oxidizing, or reducing atmosphere for periods described below.

Measurements of Doppler broadening of annihilation radiation were conducted using a slow positron beam. The beam starts with a 20 mCi ^{22}Na source, which emits positrons with energy of a few hundred keV. Using a solid Ar moderator, fast positrons are converted into few eV positrons, which are then accelerated into energies varying from 300 eV to 30 keV by biasing the target. The mean positron implantation depth z is determined using the well-known formula, $z[\text{nm}] = (40/\rho)E^{1.6}$, where ρ is the density in g/cm^3 and E is the positron energy in keV [10]. The positron lifetime measurements were conducted using the positron beam line at the Electrotechnical Laboratory. Positrons were produced by converting γ rays, generated by bombardment of 75 MeV Linac electrons on a tantalum target, into electron-positron pairs and then moderated in tungsten plates. The positron pulses are stretched in a Penning trap and rebunched with a high frequency (178 MHz) and narrow width (<300 ps).

 0031-9007/99/83(22)/4586(4)$15.00

After being implanted into a MgO sample, positrons are trapped in vacancy sites and annihilate with both valence and deeper level electrons of surrounding atoms. The annihilation photo peak is centered at 511 keV, and broadened due to the Doppler effect induced by the electron momentum. Doppler broadening can be characterized by a shape parameter S, defined as the ratio of the counts appearing in the central region to the other counts in the annihilation photo peak. The S parameter represents the contribution from annihilation with the low momentum electrons, mainly reflecting the vacancy concentration and size since the low momentum electrons dominate the electronic environment of vacancies.

Figure 1 shows the S parameter measured as a function of positron energy, corresponding to the depth shown in the top scale, for MgO samples that are as-grown, Au^+ implanted, and annealed at ~1200 °C in Ar + 5%O_2 for 90 min following implantation. For as-grown MgO, the S parameter (open circles) is mostly low, except for the near surface imperfections. After Au^+ implantation at 1.1 MeV with a dose of 6.0×10^{16} ions/cm^2, the S parameter (crosses) is greatly increased in the region between the surface and R_p. The increased S parameter indicates that a large number of vacancies is produced by implantation. The S parameter also increases for depths greater than R_p, suggesting that vacancies extend to the region beyond the reach of the Au ions due to damage by low-mass knock-on ions.

The implanted sample was annealed at ~1200 °C to promote the formation of Au nanoparticles. The S parameter increases dramatically (as shown in Fig. 1 by the solid circles). It appears that there are two peaks in the S parameter profile, separated by a valley coincident with the Au ion projected range distribution located at about 0.16–0.4 μm, as measured by RBS. At this depth, some positrons apparently annihilate with the electrons associated with the Au. The greatly increased S parameter on either side of the projected range clearly shows that the vacancies induced by implantation aggregate into larger clusters upon annealing. Two possibilities may account for the twin peaks: (1) creation of two vacancy regions by the implantation and annealing processes, or (2) formation of vacancy clusters that are attached to Au nanoparticle surfaces within R_p.

To identify a specific structure and establish the correct interpretation, positron lifetime spectra were measured for MgO samples that were prepared under the same conditions as used for the S parameter measurements. The lifetimes of trapped positrons are inversely correlated to the densities of electrons in the trapping sites, a longer lifetime indicating a larger-size vacancy cluster since the electron density in these clusters is lower than that of a smaller-size vacancy cluster. Figure 2 shows the positron lifetime spectra for 23 keV (open circles) and 5 keV (crosses) positrons bombarding an as-implanted MgO sample, and for 5 keV positrons injected into MgO at ~1200 °C for 10 h in Ar + 5%O_2 after implantation (solid circles). The spectra were analyzed by Laplace inversion (CONTIN) [11], which deconvolutes the time spectra into the probability density function (pdf), as shown in the inset of

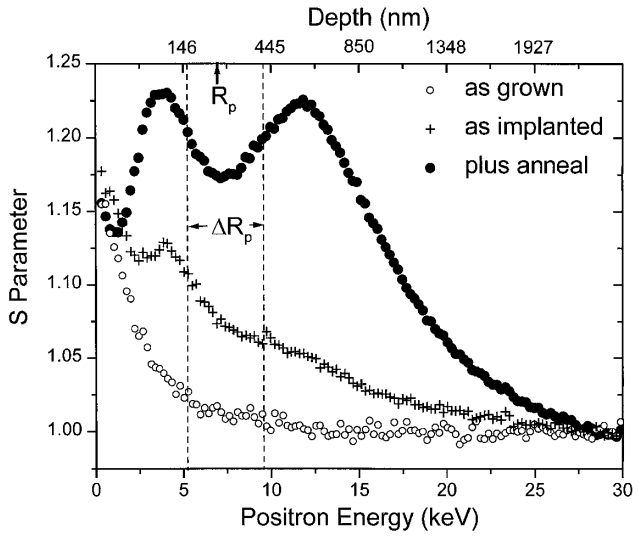

FIG. 1. S parameters as a function of positron energy for MgO samples that are as-grown (open circles), Au ion-implanted (crosses), and annealed at ~1200 °C for 90 min in Ar + 5%O_2 after implantation (solid circles). The implant parameters for high-energy implantation at 1.1 MeV with a dose of 6×10^{16} ions/cm^2. The S parameter of bulk MgO is normalized to be one.

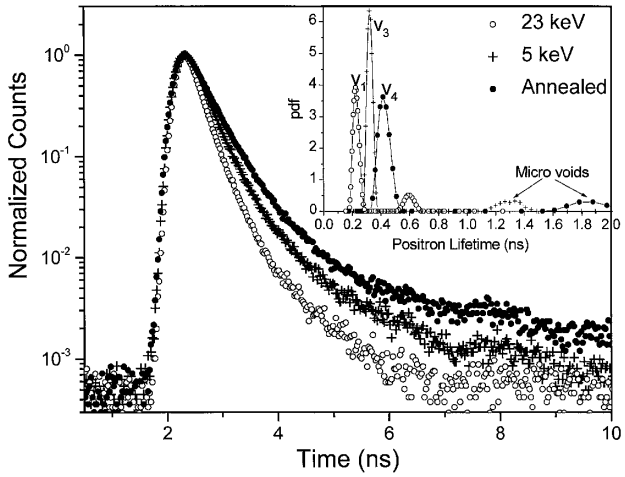

FIG. 2. Semilog plots of the counting rates as functions of the arrival time of annihilation γ rays for 23 keV (open circles) and 5 keV (crosses) positrons bombarding Au-implanted MgO, and for 5 keV of positrons injecting into MgO annealed at ~1200 °C for 10 h in Ar + 5%O_2 after implantation (solid circles). Inset: probability density functions (pdf) as a function of positron lifetime, resulting from Laplace inversion (CONTIN) of lifetime spectra. Vacancy sizes (v_1, v_3, and v_4) are determined by comparing with calculated lifetimes (Table I). The small intensity of a longer lifetime (>1 ns) suggests a small number of microvoids.

Fig. 2. The mean penetration depth of 23 keV positrons is 1.7 μm, where overlap between positrons and implanted ions is minimal. The spectrum for this energy shows a main lifetime component, 0.22 $\pm$ 0.04 ns with 89 $\pm$ 3% contribution, and a satellite component, 0.59 $\pm$ 0.07 ns with 11 $\pm$ 3% contribution. The main component is close to the lifetime of positrons trapped at single vacancies of MgO, 0.21 ns [12]. The deviation of the main lifetime from that for the perfect MgO lattice (0.16 ns) [13] and the satellite component may be due to intrinsic trapping centers in the initial as-received sample and to the positron deposition profile that overlaps with the ion-implanted region. For the lifetime spectrum of 5 keV positrons injected into the as-implanted sample, the major lifetime component increases to 0.32 $\pm$ 0.05 ns at 95 $\pm$ 3%. The mean implantation depth of 5 keV positrons is 0.15 μm, which is characteristic of the depth of the damaged region. The satellite lifetime increases to 1.32 $\pm$ 0.11 ns at 5%. After postimplantation annealing, the two lifetimes are further increased to 0.41 $\pm$ 0.08 ns at 90% and 1.8 $\pm$ 0.3 ns at 7%, respectively. Positron lifetimes for MgO defects are calculated using Puska and co-workers' model [14] in which the annihilation rates are determined by the positron density overlapping with the enhanced electron density that is proportional to the atomic polarizability of MgO. Table I lists the calculated positron lifetimes of various defects, respectively. Table I also shows the positron lifetime measured in this paper. Based on the closeness of the measured lifetimes to the calculated values, the 0.32 ns measured for as-implanted MgO is a combination of the four three-vacancy sites; the 0.41 ns measured from MgO annealed after implantation indicates that the positrons are predominantly trapped in clusters consisting of two Mg vacancies and two O vacancies. We denote these specific three- and four-vacancy clusters as "v_3" and "v_4," respectively.

TABLE I. Positron lifetimes of MgO defects calculated using the insulator model [14] and compared with the measured lifetimes. V_{Mg} and V_O mean Mg and O vacancies, respectively. V_{Mg}-V_O represents a pair of Mg and O vacancies. V_{2Mg}-V_{2O} represents a cluster consisting of two Mg and two oxygen vacancies (v_4).

Defect site	Calculated positron lifetime (ps)	Measured positron lifetime (ps)
Perfect MgO	155	160 [12]
V_O	157	...
V_{Mg}	244	210 [13]
V_{Mg}-V_O	290	...
V_{Mg}-V_{2O} (triangle)	338	300–340
V_{Mg}-V_{2O} (linear)	329	...
V_{2Mg}-V_O (triangle)	330	...
V_{2Mg}-V_O (linear)	310	...
V_{2Mg}-V_{2O}	414	375–440

The main positron lifetimes for Au-implanted and annealed MgO were measured as a function of energy (as shown in Fig. 3). After Au^+ implantation, the lifetimes within the ion damage region are longer than that for the defect-free MgO. It is important to note that, at a depth of 0.25 μm, the lifetime remains as long as those in nearby regions and no low-lifetime valley is observed. On the other hand, as shown in Fig. 1 (solid circles), the S parameter profile shows a low S-value valley at this depth. Based on the argument given below, we interpret the data as indicating that v_4 clusters are formed on Au nanoparticle surfaces (referred to as Au-v_4 complexes). In this case, positrons remain trapped in v_4 sites of the Au-v_4 complexes which apparently yield a lifetime indistinguishable from the undecorated v_4 lifetime. However, when the trapped positrons annihilate with nearby Au electrons, the S parameter is expected to be lower than that of the defected MgO bulk.

Identification of the vacancies that are attached to Au nanoparticles is confirmed by measurements of S parameter profiles as a function of an Au^+ dose for samples annealed in Ar + 5%O_2 for 90 min following implantation. As shown in Fig. 4, for a low fluence, 1×10^{16} ions/cm^2, a single broad vacancy structure covers both above and below R_p with perhaps a slight dip in S at about R_p. In this case, the S parameters within the R_p are less affected by Au implants because the Au-v_4 concentration is low, while still enough vacancy clusters are produced to trap the positrons. At a high fluence, 1×10^{17} ions/cm^2, the concentration of Au-v_4 complexes increases and therefore the S parameter is lower at about R_p. The two S parameter peaks are not due to a "twin vacancy peak," but rather an Au-v_4 "valley" is superimposed on the broad

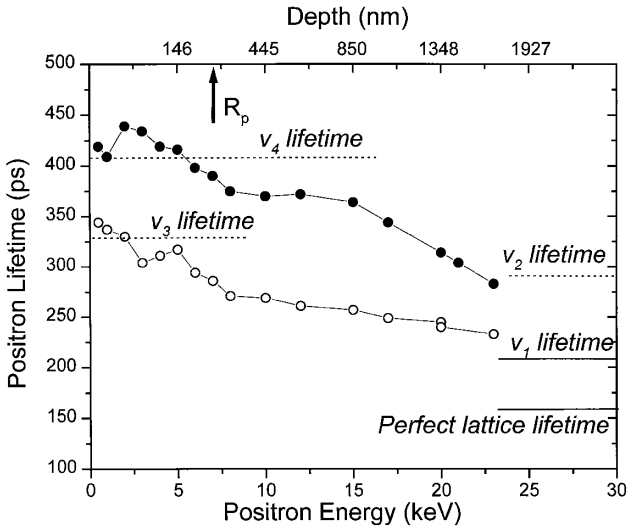

FIG. 3. Main component positron lifetimes as a function of positron energy for as-implanted (open circles) and subsequently annealed (solid circles) MgO. The implantation and annealing conditions are the same as described in Fig. 2.

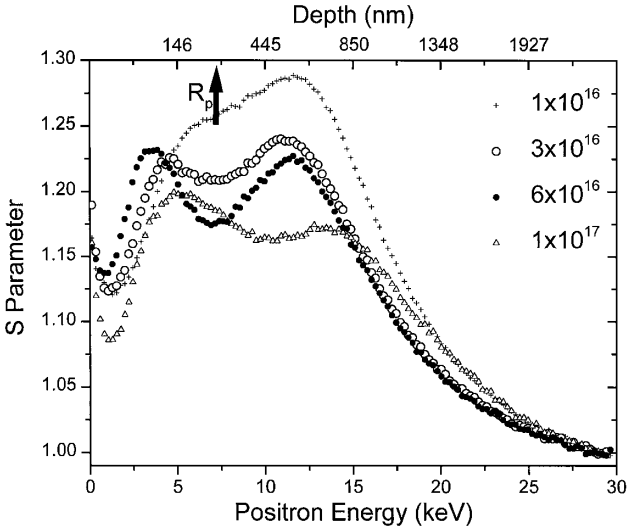

FIG. 4. S parameter as a function of positron energy for implanted and sequentially annealed MgO with fluence: 1×10^{16} Au^+/cm^2 (crosses), 3×10^{16} Au^+/cm^2 (open circles), 6×10^{16} Au^+/cm^2 (solid circles), and 1×10^{17} Au^+/cm^2 (open triangles). The implantation energy is 1.1 MeV and annealing conditions are the same as described in Fig. 1.

vacancy profile. It is noted that the S parameter for implanted samples that are not annealed (see Fig. 1, crosses) does not show the low-S parameter valley in R_p for either low or high fluence. This is because Au-v_4 complexes are not formed since the Au atoms are not fully formed into clusters and the two species are not thermally energetic enough to combine. Evidently Au nanoparticles can only be seen when they are associated with the vacancy clusters, i.e., positron traps. Our recent measurements of the high momentum part of the Doppler-broadened annihilation spectra, using the two-detector coincidence method developed by Asoka-Kumar *et al.* [15], show that the electronic momentum structure detected with positrons implanted into the Au nanoparticle layer is similar to that of an Au film. This indicates that the positrons trapped at the v_4 sites (as we know it from lifetime spectra) annihilate with the electrons associated with Au nanoparticles, which further confirms the association between the Au nanoparticle surface and the v_4 defects.

In conclusion, formation of vacancy clusters on the surfaces of Au nanoparticles embedded in MgO is observed using a combined study of variable-energy positron lifetime spectroscopy and measurements of Doppler-broadening annihilation radiation. The Au implants are not detectable until they form nanoparticles that are associated with vacancy defects. Our study also demonstrates that a positron probe can be used to characterize defect structures of nanoparticle surfaces, which is important as nanoscale fabrication becomes more prevalent.

This research is sponsored by the Division of Chemical Science of the Department of Energy under Contract No. DE-AC05-96OR22464 with Lockheed Martin Energy Research Corporation. Research at Fisk University is supported by the Department of Energy under Grant No. DE-F605-94ER45521. The authors also acknowledge support from the Science and Technology Agency of Japan, C. W. White and A. Meldrum at ORNL for implanting the MgO samples, and L. D. Hulett and B. Somieski at ORNL, R. Mu at Fisk University, and T. Ohdaira of ETL for their helpful discussions.

[1] D. Davidovic and M. Tinkham, Phys. Rev. Lett. **83**, 1644 (1999), and references therein.
[2] *Positron Spectroscopy of Solids*, edited by A. Dupasquier and A. P. Mills, Jr. (IOS Press, Amsterdam, 1995).
[3] See, for example, *Ion Beam Modification of Insulators*, edited by P. Mazzoldi and G. Arnold (Elsevier, Amsterdam, 1987).
[4] A. Ueda, R. Mu, Y. S. Tung, M. Wu, W. E. Collins, D. O. Henderson, C. W. White, R. A. Zuhr, J. D. Budai, A. Meldrum, P. W. Wang, and X. Li, Nucl. Instrum. Methods Phys. Res., Sect. B **141**, 261 (1998).
[5] R. L. Zimmerman, D. Ila, E. K. Williams, S. Sarkisov, D. B. Poker, and D. K. Hensley, Nucl. Instrum. Methods Phys. Res., Sect. B **141**, 308 (1998).
[6] C. W. White, C. J. McHargue, P. S. Sklad, L. A. Boatner, and G. C. Farlow, Mater. Sci. Rep. **4**, 43 (1989).
[7] K. Fukumi, A. Chayahara, K. Kadono, T. Sakaguchi, and Y. Hirono, J. Appl. Phys. **75**, 3075 (1994).
[8] D. O. Henderson *et al.* (to be published).
[9] B. D. Evans, J. Comas, and P. R. Malmberg, Phys. Rev. B **6**, 2453 (1972). The fact that these authors observe F_2 centers does not rule out the possibility of the coexistence of these centers with the v_4 clusters we observe.
[10] P. Asoka-Kumar, K. G. Lynn, and D. O. Welch, J. Appl. Phys. **76**, 4935 (1994).
[11] R. B. Gregory, Nucl. Instrum. Methods Phys. Res., Sect. A **302**, 496 (1991).
[12] M. Forster, W. Claudy, H. Hermes, M. Koch, K. Maier, J. Major, H. Stoll, and H.-E. Schaefer, Mater. Sci. Forum **105–110**, 1005 (1992).
[13] M. J. Puska, in *Positron Annihilation*, edited by L. Dorikens-Vanpraet, M. Dorikens, and D. Segers (World Scientific, New Jersey, 1988), p. 101.
[14] M. J. Puska, S. Makinen, M. Manninen, and R. M. Nieminen, Phys. Rev. B **39**, 7666 (1989).
[15] P. Asoka-Kumar, M. Alatalo, V. J. Ghosh, A. C. Kruseman, B. Nielsen, and K. G. Lynn, Phys. Rev. Lett. **77**, 2097 (1996).